

1 Formation of highly oxygenated organic molecules from chlorine atom  
2 initiated oxidation of alpha-pinene

3

4 Yonghong Wang<sup>1</sup>, Matthieu Riva<sup>1,2</sup>, Hongbin Xie<sup>3,1</sup>, Liine Heikkinen<sup>1</sup>, Simon  
5 Schallhart<sup>1</sup>, Qiaozhi Zha<sup>1</sup>, Chao Yan<sup>1</sup>, Xu-Cheng He<sup>1</sup>, Otso Peräkylä<sup>1</sup> and Mikael  
6 Ehn<sup>1</sup>

7

8 <sup>1</sup>Institute for Atmospheric and Earth System Research / Physics, Faculty of Science, P.  
9 O. Box 64, 00014 University of Helsinki, Helsinki, Finland

10 <sup>2</sup>Univ Lyon, Université Claude Bernard Lyon 1, CNRS, IRCELYON, F-69626,  
11 Villeurbanne, France

12 <sup>3</sup>Key Laboratory of Industrial Ecology and Environmental Engineering (MOE), School  
13 of Environmental Science and Technology, Dalian University of Technology, Dalian  
14 116024, China

15

16 Revised to: Atmospheric Chemistry and Physics

17

18 Corresponding to: Yonghong Wang and Hongbin Xie

19 [yonghong.wang@helsinki.fi](mailto:yonghong.wang@helsinki.fi); [hbxie@dlut.edu.cn](mailto:hbxie@dlut.edu.cn)

20

21

22

23

24

25

26

27

28

29

30 Abstract

31

32 Highly oxygenated organic molecules (HOMs) from atmospheric oxidation of alpha-  
33 pinene can irreversibly condense to particles and contribute to secondary organic  
34 aerosol (SOA) formation. Recently, the formation of nitryl chloride (ClNO<sub>2</sub>) from  
35 heterogeneous reactions, followed by its subsequent photolysis is suggested to be an  
36 important source of chlorine atoms in many parts of the atmosphere. However, the  
37 oxidation of monoterpenes such as alpha-pinene by chlorine atoms has received very  
38 little attention, and the ability of this reaction to form HOM is completely unstudied.  
39 Here, chamber experiments were conducted with alpha-pinene and chlorine under low  
40 and high nitrogen oxide (NO<sub>x</sub>, NO<sub>x</sub> = NO + NO<sub>2</sub>) conditions. A nitrate-based CI-API-TOF  
41 (Chemical Ionization-Atmospheric Pressure Interface-Time of Flight) was used to  
42 measure HOM products. Clear distributions of monomers with 9-10 carbon atoms and  
43 dimers with 18-20 carbon atoms were observed under low NO<sub>x</sub> conditions. With  
44 increased concentration of NO<sub>x</sub> within the chamber, the formation of dimers was  
45 suppressed due to the reactions of peroxy radicals with NO. We estimated the HOM  
46 yields from chlorine-initiated oxidation of alpha-pinene under low-NO<sub>x</sub> conditions to  
47 be around 1.8 %, though with a substantial uncertainty range (0.8-4 %) due to lack of  
48 suitable calibration methods. Corresponding yields at high NO<sub>x</sub> could not be  
49 determined because of concurrent ozonolysis reactions. Our study demonstrates that  
50 chlorine atoms also initiated oxidation of alpha-pinene and yields low volatility organic  
51 compounds.

52

53

54

55

56

57

## 58 1. Introduction

59

60 Highly oxygenated organic molecules (HOMs) have been identified as key species in  
61 the formation of new atmospheric aerosol particles and secondary organic aerosol (SOA)  
62 (Ehn et al., 2014, 2017; Kulmala et al., 2013; Bianchi et al., 2019). Recently, the  
63 formation of HOMs in the gas phase was described as an autoxidation process of peroxy  
64 radicals ( $\text{RO}_2$ ) via multiple intramolecular H atom shifts (Crouse et al., 2013; Jokinen  
65 et al., 2014b; Mentel et al., 2015; Rissanen et al., 2014). Oxygen-containing moieties  
66 such as carbonyl, carboxylic acid and hydroxyl groups can weaken nearby C-H bonds,  
67 making H-abstraction and autoxidation competitive with bimolecular  $\text{RO}_2$  reactions,  
68 e.g. with NO (Crouse et al., 2013; Praske et al., 2018). Until now, all studies on the  
69 formation of HOMs have focused on reactions initiated by oxygen-containing oxidants  
70 ( $\text{O}_3$  and OH)(Berndt et al., 2016; Ehn et al., 2014; Jokinen et al., 2015).

71

72 Increasing evidence indicates that the chlorine atom (Cl) may also play an important  
73 role in transforming atmospheric organics (Tham et al., 2016; Thornton et al., 2010).  
74 Chlorine atoms have the greatest reactivity toward volatile organic compounds (VOC),  
75 with rate constants that are, with some exceptions, an order of magnitude higher than  
76 those of hydroxyl radicals (OH) (Riva et al., 2015). Historically, chlorine atoms were  
77 thought to be formed primarily from heterogeneous reaction cycles involving sea salt,  
78 and their concentrations estimated to be around 1-10% of that of OH (Thornton et al.,  
79 2010). Therefore, the role of chlorine atoms in atmospheric oxidation processes has  
80 traditionally been thought to be limited to the marine boundary layer only. In recent  
81 years,  $\text{ClNO}_2$ , as a significant chlorine atom source, was found in continental regions  
82 of America, Canada and Germany, and high concentrations of  $\text{ClNO}_2$  were also  
83 detected in the urban atmosphere in China (Reyes-Villegas et al., 2018; Tham et al.,  
84 2016; Thornton et al., 2010; Wang et al., 2017). The new findings have expanded the  
85 potential importance of chlorine atoms from coastal areas to continental urban areas. A  
86 recent study also reported that chlorine atoms can be more important than OH radicals

87 for the oxidation of alkanes in the North China Plain (Liu et al., 2017). Therefore, it is  
88 desirable to probe the role of chlorine radicals in the degradation of VOCs and related  
89 SOA formation.

90  
91 Emission of biogenic volatile organic compounds (BVOC) to the atmosphere  
92 dominates total hydrocarbon emissions on a global scale, with methane, isoprene and  
93 terpenes having the highest source strengths (Guenther et al., 2012). Alpha-pinene is  
94 the most abundant monoterpene in the atmosphere and its oxidation products from  
95 ozonolysis and photooxidation contribute to a substantial fraction of SOA mass  
96 (Riccobono et al., 2014; Zhang et al., 2018). **Many of the regions listed earlier, where  
97 ClNO<sub>2</sub> was identified as a chlorine atom source, may also have substantial monoterpene  
98 emissions, making Cl a relevant oxidant also for BVOC.** Chlorine atom initiated  
99 reactions of alpha-pinene have also been shown to contribute to the formation of SOA,  
100 which implies that low volatile compounds are efficiently produced also in this process  
101 (Cai and Griffin, 2006; Ofner et al., 2013).

102  
103 Similar to the reaction with OH radicals, the reaction of VOCs with chlorine atoms may  
104 proceed either via addition of Cl to unsaturated bonds or via H-abstraction. Wang et al.,  
105 (2017) found that the Cl addition to isoprene can lead to the formation of low volatility  
106 organic compounds. In principle, Cl-initiated reactions could form HOMs in a similar  
107 manner as OH-initiated reactions (Berndt et al., 2016a), as the initial addition or  
108 abstraction step is comparable for both oxidants. In view of the increased understanding  
109 of the importance of chlorine atoms in atmospheric chemistry, it is desirable to  
110 investigate the formation of HOMs from reactions of common atmospheric VOC with  
111 Cl.

112  
113 Here, laboratory chamber experiments were performed to investigate the ability of  
114 chlorine atom to form HOMs from the oxidation of alpha-pinene. HOMs were  
115 characterized using a nitrate-based chemical ionization mass spectrometer, under both

116 low and high NO<sub>x</sub> conditions. The yields of these HOMs were determined under the  
117 low NO<sub>x</sub> conditions, and the atmospheric implications of this study are discussed.

118

## 119 2. Experiment and method

### 120 2.1 Experimental setup

121 The experiments were conducted in the “COALA” chamber at the University of  
122 Helsinki (Peräkylä et al., 2019; Riva et al., 2019). It is a 2 m<sup>3</sup> Teflon chamber, run as a  
123 continuously stirred tank reactor, used with a flow of 45 liter per minutes (LPM),  
124 resulting in an average residence time of about 45 minutes. The chamber is surrounded  
125 by housing to provide dark conditions. No water vapor was added to the chamber,  
126 resulting in an RH<1 %, and the temperature was the same as the temperature of the  
127 room, around 25°C. **The HOM formation targeted in this work is not expected to change**  
128 **markedly as a function of RH, as also indicated in a previous study on both ozone and**  
129 **OH initiated oxidation of monoterpenes (Li et al., 2019). Although SOA mass yields**  
130 **were not studied in this work, these may be affected by RH (Jonsson et al., 2006, 2008).**

131 A general schematic of the chamber facility is shown in Figure 1. Our experiment was  
132 aimed to probe chlorine atom initiated formation of HOMs under low/high NO<sub>x</sub>  
133 conditions. We use 400 nm LED lights to photolyze chlorine and NO<sub>2</sub> and produce  
134 chlorine atoms and NO as following:



135

136 The concentration of Cl atoms was varied by changing the amount of 400 nm light. In  
137 practice this was done by turning on different amounts of the available lights, with the  
138 maximum corresponding to seven. We will refer below to the number of lights that were  
139 turned on, although each “light” corresponds to a group of LED strips.

140

### 141 2.2 Instrumentation and data analysis

142

143 A nitrate ion ( $\text{NO}_3^-$ ) based chemical ionization atmospheric pressure interface long  
144 time-of-flight (CI-APi-L-TOF) mass spectrometer was used for measuring HOMs. The  
145 instrument has been shown to be sensitive towards this group of compounds, detecting  
146 them as adducts with the nitrate ion. Due to a lack of suitable calibration methods, the  
147 CI-APi-TOF was not calibrated for HOMs during this study. In order to estimate rough  
148 HOM concentrations ( $[\text{HOM}]$ ), we directly use the calibration coefficient  $C = 1.6 \text{ e}10$   
149  $\text{molec cm}^{-3}$  utilized by Ehn et al. (2014), to convert the measured HOM ion signals  
150 according to the equation below (Jokinen et al., 2014).

$$151 \quad [\text{HOM}] = C * \frac{\text{HOM} \cdot \text{NO}_3^-}{\text{NO}_3^- + \text{HNO}_3 \cdot \text{NO}_3^-}$$

152 This value of  $C$  is very close to values utilized in several other studies using a CI-  
153 APi-TOF (Jokinen et al., 2014, 2015; Riva et al., 2019). Ehn et al (2014) obtained their  
154 calibration factor from a permeation source using a perfluorinated acid, and also  
155 showed through calculations that there were theoretical limitations for having a much  
156 larger or a much smaller value for  $C$ .

157 This approach obviously brings large uncertainties to the HOM concentrations, which  
158 we estimate to be at least -50 %/+100 % according to previous calibration results  
159 (Jokinen et al., 2014, 2015; Riva et al., 2019). More detailed information about the  
160 instrument can be found in (Jokinen et al., 2012), noting that compared with the CI-  
161 APi-TOF used before, the long time-of-flight mass spectrometer used here has a  
162 doubled mass resolving power enabling a more accurate assignment of molecular  
163 formulas. Simultaneously, we also used a high-resolution long time-of-flight aerosol  
164 mass spectrometer (HR-L-TOF-AMS) to measure bulk aerosol chemical properties  
165 (Decarlo et al., 2006). As no seed aerosol particles were added to the chamber, the VOC  
166 oxidation products lead to new particle formation and growth to large enough sizes to  
167 be measured by the AMS. We also periodically used a filter in front of the AMS inlet to  
168 see the influence of the background signal to measured aerosol mass concentration.  
169 There were 10 minutes of filter measurements per hour during our experiments. A PTR-  
170 TOF-MS (TOF-8000, Ionicon) was used to measure the concentration of alpha-pinene  
171 in the chamber. The instrument background was determined every day for 20 mins by

172 guiding the chamber air through a catalytic converter, which removes the VOCs. Then,  
173 the background corrected signals were used to obtain alpha-pinene mixing ratios by  
174 using the calibration coefficient determined before the experiments. A description of  
175 the used setup employed for the calibration and zero air measurements have been  
176 introduced earlier (Schallhart et al., 2018). A custom-built DMPS system was used to  
177 measure the particle number size distribution from 10 nm to 400 nm in the chamber.  
178 The NO concentration was measured with an ECO-PHYSICS CLD 780 TR instrument  
179 with a detection limit of 3 ppt. NO<sub>x</sub> (=NO+NO<sub>2</sub>) concentrations were determined by  
180 using a Thermo-Fisher 42i analyzer. O<sub>3</sub> concentration was measured with a Thermo-  
181 Fisher 49i analyzer.

182

### 183 2.3 Estimation of chlorine atom concentrations

184 During steady state in the chamber, average concentrations of chlorine atom was  
185 calculated using the rate coefficients  $(4.6 \pm 1.3) \cdot 10^{-10} \text{ cm}^3 \text{ molecule}^{-1} \text{ s}^{-1}$  of Cl atoms  
186 with alpha-pinene (Finlayson-Pitts et al., 1999), as following:

$$187 \quad d[\text{AP}]/dt = Q_{\text{in}} - k * [\text{Cl}] * [\text{AP}] - Q_{\text{out}}$$

188 where Q<sub>in</sub> is the **flow rate** of alpha-pinene continuously injected into the chamber,  
189 and Q<sub>out</sub> is the **flow rate** that exited the chamber. The term Q<sub>in</sub> related  
190 **concentration** was 13.3 ppb, while the term Q<sub>out</sub> varied depending on the conditions,  
191 and is calculated as [AP]/45 min. During steady state, d[AP]/dt is zero, and then [Cl]  
192 concentration is calculated accordingly. As shown in Figure 2, the concentration of  
193 HOMs decreased and alpha-pinene increased as the number of lights switched on  
194 changed from 7 to 4, 2 and 1. We use the variation of alpha-pinene and HOM  
195 concentrations during this run to calculate both chlorine atom concentrations and HOM  
196 yields. Each change in alpha-pinene concentration was due to the change in Cl atom  
197 concentration, and with knowledge of the reaction rate, the concentration of Cl atoms  
198 as a function of the number of lights turned on was determined (Figure 3). The  
199 calculated [Cl] concentrations are in the range of  $(1-5) \times 10^5 \text{ molecules cm}^{-3}$ , which is  
200 within atmospheric relevant concentration ranges (Tham et al., 2016). Raw data from

201 the CI-API-L-TOF were recorded in 10s resolution in HDF format. We used Toftools  
202 for data analysis and detailed protocols of the software have been introduced by  
203 Junninen et al. (2010).

204

## 205 2.4 HOMs molar yield

206

207 The change of HOM concentration with time can be described as follows, in analogy  
208 with Ehn et al. (2014):

209

$$210 \frac{d[HOMs]}{dt} = k_1 g [\alpha - pinene][Cl] - k_{loss}[HOMs] \quad (1)$$

211

212

$$213 g = \frac{k_{loss}[HOMs]}{k_1[\alpha - pinene][Cl]} \quad (2)$$

214

215 Here,  $k_1$  is the reaction rate coefficient of alpha-pinene with chlorine atoms and  $\gamma$  is the  
216 molar yield of HOMs, i.e., the fraction of alpha-pinene + Cl reactions that produced  
217 HOMs.  $k_{loss}$  is the loss rate of HOMs to the chamber walls and particles, though the  
218 latter was negligible in this study due to the low aerosol loadings. We used 300 s as a  
219 lifetime of HOMs, i.e.  $k_{loss} = 1/300 \text{ s}^{-1}$ , in our previous study in the COALA chamber  
220 (Riva et al., 2019).

221

## 222 3. Results and discussion

### 223 3.1 Formation of HOMs under low NO condition

224

225 Figure 4 (a, b, c and d) shows mass spectra measured by the NO<sub>3</sub>-CI-API-TOF during  
226 steady state alpha-pinene oxidation with different amounts of lights switched on. The



227 x-axis represents mass to charge ratio, in units of Thomson (Th). The y-axis represents  
228 signals in units of counts per second. As we can see, both monomers (280-400 Th) and  
229 dimers (440-580 Th) showed increased signals with increased number of lights, and  
230 consequently increased [Cl]. The most abundant peaks are labeled in Figure 4d, with  
231 some of the largest signals in the monomer range attributed to  $C_9H_{12}O_{7,8}$  and  
232  $C_{10}H_{14}O_{8,9,10}$ . The formation of both groups could correspond to the oxidation being initiated by H-  
233 atom abstraction by Cl, and final termination (from uni- or bimolecular reactions) leading to loss of  
234 OH or HO<sub>2</sub>. For the C<sub>9</sub> compounds, an additional loss of formaldehyde (CH<sub>2</sub>O) during the oxidation  
235 process would explain the amount of observed C and H atoms. During the oxidation of C<sub>10</sub>H<sub>16</sub>,  
236 in the absence of NO, the fate of RO<sub>2</sub> radicals depends on the concentrations of HO<sub>2</sub>  
237 and RO<sub>2</sub>. Autoxidation competes with bimolecular reactions, becoming more likely at  
238 lower RO<sub>2</sub> and HO<sub>2</sub> concentrations.

239

240 As we show in the Figure 4(d),  $C_{10}H_{14}O_{8-12}$  compounds are large peaks in the monomer  
241 range observed with the NO<sub>3</sub>-Cl-API-TOF. These compounds with 14 hydrogens may  
242 come from decomposition of  $C_{10}H_{15}O_n$  peroxy radicals via loss of OH or HO<sub>2</sub>, or  
243 following reactions with other RO<sub>2</sub>, as depicted schematically in Figure 5. Another  
244 abundant group is  $C_{10}H_{16}O_{6-12}$ , which may result from RO<sub>2</sub> terminated by HO<sub>2</sub>. In the  
245 dimer range, the most abundant compounds are  $C_{19}H_{28}O_{8-14}$  and  $C_{20}H_{30}O_{11-14}$ . These  
246 compounds come from RO<sub>2</sub> cross reactions, as has been shown in multiple earlier  
247 studies (Ehn et al., 2014b; Jokinen et al., 2015; Mentel et al., 2015). The  $C_{20}H_{30}O_n$   
248 dimers are most likely formed from reactions of two  $C_{10}H_{15}O_x$  radicals, as were many  
249 abundant monomers. As noted earlier, Cl oxidation of alkenes may occur via a Cl  
250 addition (forming an initial radical containing 16 H-atoms and one Cl atom) or via an  
251 H-abstraction reaction (forming a radical with 15 H-atoms and no Cl) (Figure 5). The  
252 abstraction pathway leads to HOM formation, or the Cl atom is lost during the  
253 subsequent reaction in the oxidation processes. With our data, we cannot rule out either  
254 of these explanations for this result. Loss of HCl from alpha-pinene products from Cl  
255 oxidation have, to our knowledge, only been reported to take place in the aerosol phase

256 (Ofner et al., 2013).

257

258 Figure 6 shows the variation of several close-shelled HOM products and the peroxy  
259 radical  $C_{10}H_{15}O_{10}$  measured by  $NO_3$ -CI-API-TOF when we changed the lights from  
260 dark conditions to 1, 2, 4 and 7 lights switched on. Given the low Cl atom concentration,  
261 it is expected that no multi-generation oxidation by Cl can take place, and the behavior  
262 of all closed shell oxidation products should follow similar patterns. As seen in Figure  
263 6, this was the case both for monomers and dimers. The less steep increase of the radical  
264 is also according to expectations, as the formation of  $RO_2$  is linear with the alpha-pinene  
265 oxidation rate, but the loss rate (when dominated by  $RO_2$  cross reactions) is proportional  
266 to  $(RO_2)^2$ . For closed shell species, the wall loss-driven loss rate stays constant  
267 throughout the experiment, and therefore they increase linearly with the alpha-pinene  
268 oxidation rate while the  $RO_2$  radicals increase as the square root of the oxidation rate.  
269 For more detailed discussion on  $RO_2$  dynamics in a steady state chamber, see Ehn et al.  
270 (2014).

271

272 In Figure7, we plotted time series of the particle number size distribution and the total  
273 number concentration, together with mass concentrations of particulate chloride and  
274 organics as we changed the number of lights. Particle formation was detected even at  
275 the lowest Cl atom concentration, as indicated by the increases in aerosol number  
276 concentration. An increase in aerosol mass concentration as detected by the AMS only  
277 took place at the two highest Cl atom concentrations, when the particles were able to  
278 grow into a size range measurable by the AMS. Particulate chloride mass  
279 concentrations also increased relatively linearly with the concentration of organics as  
280 we increased the number of lights. The Chl/Org ratio was only around 3 %, suggesting  
281 that the majority of condensed OVOC did not contain Cl atoms. However, the exact Chl  
282 quantification from organochlorides using the AMS may contain uncertainties (Wang and Ruiz,  
283 2017), and we avoid drawing too far-reaching conclusions from this value, keeping also in mind  
284 that some fraction of the size distribution was below the lowest detectable size of our AMS. In

285 addition, some part of the chloride signal may also result from adsorption of HCl to  
286 particles.

287

### 288 3.2 Formation of HOMs at high NO<sub>x</sub>

289

290 Anthropogenic emissions have a significant influence on the formation of SOA, to a  
291 large part due to the influence of NO<sub>x</sub> on the atmospheric oxidation chemistry (Lee et  
292 al., 2016). In general, the fate of peroxy radicals in chamber experiments can be  
293 dominated by reactions with other RO<sub>2</sub>, HO<sub>2</sub> or NO, depending on the exact conditions.  
294 In our experiments without NO<sub>x</sub> addition, RO<sub>2</sub> was expected to be the main terminator,  
295 as also supported by the high number of detected ROOR dimers. In the atmosphere, all  
296 of the three mentioned reaction partners may be relevant at the same time. However,  
297 with increased anthropogenic influence, the reaction of RO<sub>2</sub> with NO will often become  
298 dominant. Therefore, we added NO<sub>x</sub> to the chamber as it allowed for the isolation of  
299 the formation pathways leading to HOMs in cases where NO was the main terminator  
300 for RO<sub>2</sub> radicals. Figure 8 depicts a HOM mass spectrum at steady state during alpha-  
301 pinene oxidation by chlorine radicals in the presence of ~10 ppb NO<sub>x</sub>, with the  
302 maximum 7 lights turned on. As anticipated, the dimers above 440 Th were greatly  
303 reduced compared to the runs without NO<sub>x</sub>. As more lights were turned on, both the Cl  
304 atoms and NO formation increased, as the 400 nm lights photolyze both Cl<sub>2</sub> and NO<sub>2</sub>.  
305 This coupling, together with the fact that the NO<sub>2</sub> photolysis leads to ozone formation,  
306 which subsequently can react with alpha-pinene to form HOMs, limits our quantitative  
307 analysis of these experiments. However, we conclude that efficient HOM formation  
308 took place also under these high-NO<sub>x</sub> conditions, and thus the autoxidation occurs  
309 rapidly enough to still compete with RO<sub>2</sub> termination reactions. The NO<sub>x</sub> addition also  
310 formed an abundance of organonitrate compounds like C<sub>10</sub>H<sub>15</sub>NO<sub>8,9,10,11,12</sub>, as shown in  
311 Figure 8. This family of compounds may also form from H-abstraction by the chlorine  
312 radical, followed by autoxidation and finally radical termination by NO. We calculated  
313 reacted alpha-pinene from ozone and Chlorine atom as following:  $[AP_{\text{ozone}}]/[AP_{\text{Cl}}]$

314  $=[\text{AP}][\text{Ozone}]2.5 \times 10^4 k_{\text{ap+ozone}}/[\text{AP}][\text{Cl}]k_{\text{ap+Cl}}$ , the result is around 0.2. With the results, we  
315 conclude that alpha-pinene reaction with chlorine atom is the main reaction in the system.

316 The concurrent formation of ozone means that also some alpha-pinene ozonolysis  
317 reaction will take place, though oxidation by Cl atoms was still the main loss for alpha-  
318 pinene also under these conditions.

319

320 Figure 9 shows variation of some nitrogen-containing HOMs and variation of alpha-  
321 pinene, ozone, NO and NO<sub>x</sub>, as we changed the lights from dark conditions to 1, 2, 4  
322 or 7 lights switched on. The concentrations of alpha-pinene and NO<sub>2</sub> decreased because  
323 of the consumption by chlorine radicals and photolysis of NO<sub>2</sub> into NO. Importantly,  
324 we did not observe any SOA when we had NO in the chamber. NO may have suppressed  
325 the particle formation by suppressing the dimer formation, as these have been shown to  
326 be important for initial particle formation (Tröstl et al., 2016).

327

### 328 3.3 Estimated HOMs production yields

329

330 Quantifying the molar yields of HOMs is essential to know their potential importance  
331 from a specific system. We attempt to estimate the molar yield in the case of Cl  
332 oxidation of alpha-pinene in the absence of NO<sub>x</sub>. The initial C<sub>10</sub>H<sub>16</sub> concentration is  
333 around 13.3 ppb without any UV lights switched on in the chamber. As we changed the  
334 lights, alpha-pinene and HOM concentrations varied as we showed in Figure 3. In  
335 addition, we calculated the concentration of Cl radicals as introduced in the Methods  
336 section. With this information, we can calculate the formation rate of HOM, which in  
337 steady state equals the HOM loss rate  $[\text{HOM}]k_{\text{loss}}$ . We can also calculate the oxidation  
338 rate of alpha-pinene as  $[\text{alpha-pinene}][\text{Cl}]k_{\text{AP+Cl}}$ . The ratio of these two numbers  
339 corresponds to the HOM molar yield. We selected the same runs as in Fig. 3, used also  
340 for calculating the chlorine radical concentration, and calculated the ratio as a linear fit  
341 to these four conditions (Figure 10). We get a slope of 0.018, meaning a HOM yield of  
342 1.8%. Considering the uncertainty in estimating absolute HOM concentrations, we

343 conservatively estimate that the molar HOM yield from alpha-pinene + Cl is within the  
344 range of 0.8-4 %. These values are similar to HOM yields reported for alpha-pinene  
345 oxidation by ozone and OH (Berndt et al., 2016; Ehn et al., 2014).

346

#### 347 4.Conclusion

348

349 We have systematically explored the reactions of alpha-pinene with chlorine atoms in  
350 a simulation smog chamber under atmospherically relevant conditions. We measured  
351 substantial amounts of highly oxidized organic molecules (HOM) with a NO<sub>3</sub>-Cl-API-  
352 TOF. With increasing UV lights, and consequently higher chlorine radical  
353 concentrations, the concentrations of both HOM and secondary organic aerosol  
354 increased. With addition of NO<sub>x</sub>, HOM monomer formation was still efficient, but the  
355 particle formation decreased greatly. We estimated HOM molar yields of around 1.8 %  
356 (0.8-4 %) from the reaction of alpha-pinene with Cl atoms. Our study thus indicates  
357 that in regions where chlorine atom oxidation is of importance, its possible reactions  
358 with monoterpenes can be an important source of HOM, and consequently, SOA.

359

#### 360 **Acknowledgement**

361 This work is supported by European Research Council (Grant 638703-COALA)  
362 project and Academy of Finland, via the Center of Excellence in Atmospheric Sciences  
363 and project numbers 317380 and 320094. We acknowledge the Toftools team for  
364 providing the software.

365

#### 366 **Competing financial interests**

367 The authors declare no competing financial interests.

368

369 **Author contributions**

370 Y. H. W, H. B. X and M. E had the original idea of the study. Y. H. W, M. R and H. B.

371 X conducted the chamber experiments. Y. H. W, M. R, H. B. X, L.H and M. E

372 interpreted the data. Y.H.W plotted the figures, wrote the manuscript with comments

373 and suggestions from all co-authors.

374

375

376

377

378

379

380

381

382

383

384

385

386

387 **Reference**

388 Berndt, T., Richters, S., Jokinen, T., Hyttinen, N., Kurtén, T., Otkjaer, R. V,

389 Kjaergaard, H. G., Stratmann, F., Herrmann, H., Sipilä, M., Kulmala, M. and Ehn, M.:  
390 ARTICLE Hydroxyl radical-induced formation of highly oxidized organic  
391 compounds, , doi:10.1038/ncomms13677, 2016a.

392 Berndt, T., Richters, S., Jokinen, T., Hyttinen, N., Kurtén, T., Otkjær, R. V.,  
393 Kjaergaard, H. G., Stratmann, F., Herrmann, H., Sipilä, M., Kulmala, M. and Ehn, M.:  
394 Hydroxyl radical-induced formation of highly oxidized organic compounds, Nature  
395 Communications, 7, 13677 [online] Available from:  
396 <https://doi.org/10.1038/ncomms13677>, 2016b.

397 Bianchi, F., Kurtén, T., Riva, M., Mohr, C., Rissanen, M. P., Roldin, P., Berndt, T.,  
398 Crouse, J. D., Wennberg, P. O., Mentel, T. F., Wildt, J., Junninen, H., Jokinen, T.,  
399 Kulmala, M., Worsnop, D. R., Thornton, J. A., Donahue, N., Kjaergaard, H. G. and  
400 Ehn, M.: Highly Oxygenated Organic Molecules (HOM) from Gas-Phase  
401 Autoxidation Involving Peroxy Radicals: A Key Contributor to Atmospheric Aerosol,  
402 Chemical Reviews, 119(6), 3472–3509, doi:10.1021/acs.chemrev.8b00395, 2019.

403 Cai, X. and Griffin, R. J.: Secondary aerosol formation from the oxidation of biogenic  
404 hydrocarbons by chlorine atoms, Journal of Geophysical Research Atmospheres,  
405 111(14), 1–14, doi:10.1029/2005JD006857, 2006.

406 Crouse, J. D., Nielsen, L. B., Jørgensen, S., Kjaergaard, H. G. and Wennberg, P. O.:  
407 Autoxidation of organic compounds in the atmosphere, Journal of Physical Chemistry  
408 Letters, 4(20), 3513–3520, doi:10.1021/jz4019207, 2013.

409 Decarlo, P. F., Kimmel, J. R., Trimborn, A., Northway, M. J., Jayne, J. T., Aiken, A.  
410 C., Gonin, M., Fuhrer, K., Horvath, T., Docherty, K. S., Worsnop, D. R. and Jimenez,  
411 J. L.: Field-Deployable, High-Resolution, Time-of-Flight Aerosol Mass Spectrometer,  
412 Analytical Chemistry, 78, 8281–8289, doi:10.1021/ac061249n, 2006.

413 Ehn, M., Thornton, J. A., Kleist, E., Sipilä, M., Junninen, H., Pullinen, I., Springer,  
414 M., Rubach, F., Tillmann, R., Lee, B., Lopez-Hilfiker, F., Andres, S., Acir, I.-H.,  
415 Rissanen, M., Jokinen, T., Schobesberger, S., Kangasluoma, J., Kontkanen, J.,  
416 Nieminen, T., Kurtén, T., Nielsen, L. B., Jørgensen, S., Kjaergaard, H. G.,  
417 Canagaratna, M., Maso, M. D., Berndt, T., Petäjä, T., Wahner, A., Kerminen, V.-M.,

418 Kulmala, M., Worsnop, D. R., Wildt, J. and Mentel, T. F.: A large source of low-  
419 volatility secondary organic aerosol, *Nature*, 506(7489), 476–479,  
420 doi:10.1038/nature13032, 2014a.

421 Ehn, M., Thornton, J. A., Kleist, E., Sipilä, M., Junninen, H., Pullinen, I., Springer,  
422 M., Rubach, F., Tillmann, R., Lee, B., Lopez-Hilfiker, F., Andres, S., Acir, I.-H.,  
423 Rissanen, M., Jokinen, T., Schobesberger, S., Kangasluoma, J., Kontkanen, J.,  
424 Nieminen, T., Kurtén, T., Nielsen, L. B., Jørgensen, S., Kjaergaard, H. G.,  
425 Canagaratna, M., Dal Maso, M., Berndt, T., Petäjä, T., Wahner, A., Kerminen, V.-M.,  
426 Kulmala, M., Worsnop, D. R., Wildt, J. and Mentel, T. F.: A large source of low-  
427 volatility secondary organic aerosol, *Nature*, 506, doi:10.1038/nature13032, 2014b.

428 Ehn, M., Berndt, T., Wildt, U. and Mentel, T.: Highly Oxygenated Molecules from  
429 Atmospheric Autoxidation of Hydrocarbons: A Prominent Challenge for Chemical  
430 Kinetics Studies, *International journal of chemical kinetics*, 821–831,  
431 doi:10.1002/kin.21130, 2017.

432 Finlayson-Pitts, B. J., Keoshian, C. J., Buehler, B. and Ezell, A. A.: Kinetics of  
433 Reaction of Chlorine Atoms with Some, *International Journal of Chemical Kinetics*,  
434 31, 491–499, 1999.

435 Guenther, A., Hewitt, C. N., Erickson, D., Fall, R., Geron, C., Graedel, T., Harley, P.,  
436 Klinger, L., Lerdau, M., McKay, W. A., Pierce, T., Scholes, B., Steinbrecher, R.,  
437 Tallamraju, R., Taylor, J. and Zimmerman, P.: A global model of natural volatile  
438 organic compound emissions, *Journal of Geophysical Research: Atmospheres*,  
439 100(D5), 8873–8892, doi:10.1029/94JD02950, 1995.

440 Jokinen, T., Sipilä, M., Junninen, H., Ehn, M., Lönn, G., Hakala, J., Petäjä, T.,  
441 Mauldin Iii, R. L., Kulmala, M. and Worsnop, D. R.: Atmospheric sulphuric acid and  
442 neutral cluster measurements using CI-APi-TOF, *Atmos. Chem. Phys. Atmospheric  
443 Chemistry and Physics*, 12, 4117–4125, doi:10.5194/acp-12-4117-2012, 2012.

444 Jokinen, T., Sipilä, M., Richters, S., Kerminen, V., Paasonen, P., Stratmann, F.,  
445 Worsnop, D., Kulmala, M., Ehn, M., Herrmann, H. and Berndt, T.: Rapid  
446 Autoxidation Forms Highly Oxidized RO<sub>2</sub> Radicals in the Atmosphere \*\*



447 Angewandte, , 1–6, doi:10.1002/anie.201408566, 2014a.

448 Jokinen, T., Sipilä, M., Richters, S., Kerminen, V. M., Paasonen, P., Stratmann, F.,  
449 Worsnop, D., Kulmala, M., Ehn, M., Herrmann, H. and Berndt, T.: Rapid  
450 autoxidation forms highly oxidized RO<sub>2</sub> radicals in the atmosphere, Angewandte  
451 Chemie - International Edition, 53(52), 14596–14600, doi:10.1002/anie.201408566,  
452 2014b.

453 Jokinen, T., Berndt, T., Makkonen, R., Kerminen, V.-M., Junninen, H., Paasonen, P.,  
454 Stratmann, F., Herrmann, H., Guenther, A. B., Worsnop, D. R., Kulmala, M., Ehn, M.  
455 and Sipilä, M.: Production of extremely low volatile organic compounds from  
456 biogenic emissions: Measured yields and atmospheric implications, Proceedings of  
457 the National Academy of Sciences, 112(23), 7123–7128,  
458 doi:10.1073/pnas.1423977112, 2015.

459 Jonsson, Å. M., Hallquist, M. and Ljungström, E.: Impact of humidity on the ozone  
460 initiated oxidation of limonene,  $\Delta^3$ -carene, and  $\alpha$ -pinene, Environmental Science and  
461 Technology, 40(1), 188–194, doi:10.1021/es051163w, 2006.

462 Jonsson, Å. M., Hallquist, M. and Ljungström, E.: Influence of OH scavenger on the  
463 water effect on secondary organic aerosol formation from ozonolysis of limonene,  
464  $\Delta^3$ -carene, and  $\alpha$ -pinene, Environmental Science and Technology, 42(16), 5938–  
465 5944, doi:10.1021/es702508y, 2008.

466 Kulmala, M., Kontkanen, J., Junninen, H., Lehtipalo, K., Manninen, H. E., Nieminen,  
467 T., Petäjä, T., Sipilä, M., Schobesberger, S., Rantala, P., Franchin, A., Jokinen, T.,  
468 Järvinen, E., Äijälä, M., Kangasluoma, J., Hakala, J., Aalto, P. P., Paasonen, P.,  
469 Mikkilä, J., Vanhanen, J., Aalto, J., Hakola, H., Makkonen, U., Ruuskanen, T.,  
470 Mauldin, R. L., Duplissy, J., Vehkamäki, H., Bäck, J., Kortelainen, A., Riipinen, I.,  
471 Kurtén, T., Johnston, M. V., Smith, J. N., Ehn, M., Mentel, T. F., Lehtinen, K. E. J.,  
472 Laaksonen, A., Kerminen, V. M. and Worsnop, D. R.: Direct observations of  
473 atmospheric aerosol nucleation, Science, 339(6122), 943–946,  
474 doi:10.1126/science.1227385, 2013.

475 Lee, B. H., Mohr, C., Lopez-Hilfiker, F. D., Lutz, A., Hallquist, M., Lee, L., Romer,

476 P., Cohen, R. C., Iyer, S., Kurtén, T., Hu, W., Day, D. A., Campuzano-Jost, P.,  
477 Jimenez, J. L., Xu, L., Ng, N. L., Guo, H., Weber, R. J., Wild, R. J., Brown, S. S.,  
478 Koss, A., de Gouw, J., Olson, K., Goldstein, A. H., Seco, R., Kim, S., McAvey, K.,  
479 Shepson, P. B., Starn, T., Baumann, K., Edgerton, E. S., Liu, J., Shilling, J. E., Miller,  
480 D. O., Brune, W., Schobesberger, S., D'Ambro, E. L. and Thornton, J. A.: Highly  
481 functionalized organic nitrates in the southeast United States: Contribution to  
482 secondary organic aerosol and reactive nitrogen budgets, *Proceedings of the National*  
483 *Academy of Sciences*, 113(6), 1516–1521, doi:10.1073/pnas.1508108113, 2016.

484 Li, X., Chee, S., Hao, J., Abbatt, J. P. D., Jiang, J. and Smith, J. N.: Relative humidity  
485 effect on the formation of highly oxidized molecules and new particles during  
486 monoterpene oxidation, *Atmospheric Chemistry and Physics*, 19(3), 1555–1570,  
487 doi:10.5194/acp-19-1555-2019, 2019.

488 Liu, X., Qu, H., Huey, L. G., Wang, Y., Sjostedt, S., Zeng, L., Lu, K., Wu, Y., Hu,  
489 M., Shao, M., Zhu, T. and Zhang, Y.: High Levels of Daytime Molecular Chlorine  
490 and Nitryl Chloride at a Rural Site on the North China Plain, *Environ Sci Technol*, 51,  
491 9588–9595, doi:10.1021/acs.est.7b03039, 2017.

492 Mentel, T. F., Springer, M., Ehn, M., Kleist, E., Pullinen, I., Kurtén, T., Rissanen, M.,  
493 Wahner, A. and Wildt, J.: Formation of highly oxidized multifunctional compounds:  
494 autoxidation of peroxy radicals formed in the ozonolysis of alkenes – deduced from  
495 structure–product relationships, *Atmos. Chem. Phys*, 15, 6745–6765,  
496 doi:10.5194/acp-15-6745-2015, 2015.

497 Ofner, J., Kamilli, K. A., Held, A., Lendl, B. and Zetzsch, C.: Halogen-induced  
498 organic aerosol (XOA): a study on ultra-fine particle formation and time-resolved  
499 chemical characterization, *Faraday Discussions*, 165, 135, doi:10.1039/c3fd00093a,  
500 2013.

501 Peräkylä, O., Riva, M., Heikkinen, L., Quéléver, L., Roldin, P. and Ehn, M.:  
502 Experimental investigation into the volatilities of highly oxygenated organic  
503 molecules ( HOM ), , (July), 1–28, 2019.

504 Praske, E., Otkjær, R. V, Crouse, J. D., Hethcox, J. C., Stoltz, B. M., Kjaergaard, H.

505 G. and Wennberg, P. O.: Atmospheric autoxidation is increasingly important in urban  
506 and suburban North America, *Proceedings of the National Academy of Sciences*,  
507 115(1), 64 LP – 69, doi:10.1073/pnas.1715540115, 2018.

508 Reyes-Villegas, E., Priestley, M., Ting, Y.-C., Haslett, S., Bannan, T., Le Breton, M.,  
509 Williams, P. I., Bacak, A., Flynn, M. J., Coe, H., Percival, C. and Allan, J. D.:  
510 Simultaneous aerosol mass spectrometry and chemical ionisation mass spectrometry  
511 measurements during a biomass burning event in the UK: insights into nitrate  
512 chemistry, *Atmos. Chem. Phys.*, 185194, 4093–4111, doi:10.5194/acp-18-4093-2018,  
513 2018.

514 Riccobono, F., Schobesberger, S., Scott, C. E., Dommen, J., Ortega, I. K., Rondo, L.,  
515 Almeida, J., Amorim, A., Bianchi, F., Breitenlechner, M., David, A., Downard, A.,  
516 Dunne, E. M., Duplissy, J., Ehrhart, S., Flagan, R. C., Franchin, A., Hansel, A.,  
517 Junninen, H., Kajos, M., Keskinen, H., Kupc, A., Kürten, A., Kvashin, A. N.,  
518 Laaksonen, A., Lehtipalo, K., Makhmutov, V., Mathot, S., Nieminen, T., Onnela, A.,  
519 Petäjä, T., Praplan, A. P., Santos, F. D., Schallhart, S., Seinfeld, J. H., Sipilä, M.,  
520 Spracklen, D. V, Stozhkov, Y., Stratmann, F., Tomé, A., Tsagkogeorgas, G.,  
521 Vaattovaara, P., Viisanen, Y., Vrtala, A., Wagner, P. E., Weingartner, E., Wex, H.,  
522 Wimmer, D., Carslaw, K. S., Curtius, J., Donahue, N. M., Kirkby, J., Kulmala, M.,  
523 Worsnop, D. R. and Baltensperger, U.: Oxidation Products of Biogenic Emissions  
524 Contribute to Nucleation of Atmospheric Particles, *Science*, 344(717),  
525 doi:10.1126/science.1243527, 2014.

526 Rissanen, M. P., Kurtén, T., Sipilä, M., Thornton, J. A., Kangasluoma, J., Sarnela, N.,  
527 Junninen, H., Jørgensen, S., Schallhart, S., Kajos, M. K., Taipale, R., Springer, M.,  
528 Mentel, T. F., Ruuskanen, T., Petäjä, T., Worsnop, D. R., Kjaergaard, H. G. and Ehn,  
529 M.: The formation of highly oxidized multifunctional products in the ozonolysis of  
530 cyclohexene, *Journal of the American Chemical Society*, 136(44), 15596–15606,  
531 doi:10.1021/ja507146s, 2014.

532 Riva, M., Healy, R. M., Flaud, P. M., Perraudin, E., Wenger, J. C. and Villenave, E.:  
533 Gas- and Particle-Phase Products from the Chlorine-Initiated Oxidation of Polycyclic

534 Aromatic Hydrocarbons, *Journal of Physical Chemistry A*, 119(45), 11170–11181,  
535 doi:10.1021/acs.jpca.5b04610, 2015.

536 Riva, M., Heikkinen, L., Bell, D. M., Peräkylä, O., Zelenyuk, A. and Ehn, M.:  
537 Chemical transformations in monoterpene-derived organic aerosol enhanced by  
538 inorganic composition, *npj Climate and Atmospheric Science*, (July 2018), 1–9,  
539 doi:10.1038/s41612-018-0058-0, 2019a.

540 Riva, M., Rantala, P., Krechmer, E. J., Peräkylä, O., Zhang, Y., Heikkinen, L.,  
541 Garmash, O., Yan, C., Kulmala, M., Worsnop, D. and Ehn, M.: Evaluating the  
542 performance of five different chemical ionization techniques for detecting gaseous  
543 oxygenated organic species, *Atmospheric Measurement Techniques*, 12(4), 2403–  
544 2421, doi:10.5194/amt-12-2403-2019, 2019b.

545 Schallhart, S., Rantala, P., Kajos, M. K., Aalto, J., Mammarella, I., Ruuskanen, T. M.  
546 and Kulmala, M.: Temporal variation of VOC fluxes measured with PTR-TOF above  
547 a boreal forest, *Atmospheric Chemistry and Physics*, 18(2), 815–832,  
548 doi:10.5194/acp-18-815-2018, 2018.

549 Tham, Y. J., Wang, Z., Li, Q., Yun, H., Wang, W., Wang, X., Xue, L., Lu, K., Ma, N.,  
550 Bohn, B., Li, X., Kecorius, S., Größ, J., Shao, M., Wiedensohler, A., Zhang, Y. and  
551 Wang, T.: Significant concentrations of nitryl chloride sustained in the morning:  
552 investigations of the causes and impacts on ozone production in a polluted region of  
553 northern China, *Atmos. Chem. Phys*, 16, 14959–14977, doi:10.5194/acp-16-14959-  
554 2016, 2016.

555 Thornton, J. A., Kercher, J. P., Riedel, T. P., Wagner, N. L., Cozic, J., Holloway, J.  
556 S., Dubé, W. P., Wolfe, G. M., Quinn, P. K., Middlebrook, A. M., Alexander, B. and  
557 Brown, S. S.: A large atomic chlorine source inferred from mid-continental reactive  
558 nitrogen chemistry, *Nature*, 464(7286), 271–274, doi:10.1038/nature08905, 2010a.

559 Thornton, J. A., Kercher, J. P., Riedel, T. P., Wagner, N. L., Cozic, J., Holloway, J.  
560 S., Dubé, W. P., Wolfe, G. M., Quinn, P. K., Middlebrook, A. M., Alexander, B. and  
561 Brown, S. S.: A large atomic chlorine source inferred from mid-continental reactive  
562 nitrogen chemistry, *Nature*, 464(7286), 271–274, doi:10.1038/nature08905, 2010b.

563 Tröstl, J., Chuang, W. K., Gordon, H., Heinritzi, M., Yan, C., Molteni, U., Ahlm, L.,  
564 Frege, C., Bianchi, F., Wagner, R., Simon, M., Lehtipalo, K., Williamson, C., Craven,  
565 J. S., Duplissy, J., Adamov, A., Almeida, J., Bernhammer, A.-K., Breitenlechner, M.,  
566 Brilke, S., Dias, A., Ehrhart, S., Flagan, R. C., Franchin, A., Fuchs, C., Guida, R.,  
567 Gysel, M., Hansel, A., Hoyle, C. R., Jokinen, T., Junninen, H., Kangasluoma, J.,  
568 Keskinen, H., Kim, J., Krapf, M., Kürten, A., Laaksonen, A., Lawler, M., Leiminger,  
569 M., Mathot, S., Möhler, O., Nieminen, T., Onnela, A., Petäjä, T., Piel, F. M.,  
570 Miettinen, P., Rissanen, M. P., Rondo, L., Sarnela, N., Schobesberger, S., Sengupta,  
571 K., Sipilä, M., Smith, J. N., Steiner, G., Tomè, A., Virtanen, A., Wagner, A. C.,  
572 Weingartner, E., Wimmer, D., Winkler, P. M., Ye, P., Carslaw, K. S., Curtius, J.,  
573 Dommen, J., Kirkby, J., Kulmala, M., Riipinen, I., Worsnop, D. R., Donahue, N. M.  
574 and Baltensperger, U.: The role of low-volatility organic compounds in initial particle  
575 growth in the atmosphere, *Nature*, 533(7604), 527–531, doi:10.1038/nature18271,  
576 2016.

577 Wang, D. S. and Ruiz, L. H.: Secondary organic aerosol from chlorine-initiated  
578 oxidation of isoprene, *Atmospheric Chemistry and Physics*, 17(22), 13491–13508,  
579 doi:10.5194/acp-17-13491-2017, 2017.

580 Wang, Z., Wang, W., Tham, Y. J., Li, Q., Wang, H., Wen, L., Wang, X. and Wang,  
581 T.: Fast heterogeneous  $\text{N}_2\text{O}_5$  uptake and  $\text{ClNO}_2$  production in power plant and  
582 industrial plumes observed in the nocturnal residual layer over the North China Plain,  
583 *Atmos. Chem. Phys.*, 17(19), 12361–12378, doi:10.5194/acp-17-12361-2017, 2017.

584 Zhang, H., Yee, L. D., Lee, B. H., Curtis, M. P., Worton, D. R., Isaacman-VanWertz,  
585 G., Offenberg, J. H., Lewandowski, M., Kleindienst, T. E., Beaver, M. R., Holder, A.  
586 L., Lonneman, W. A., Docherty, K. S., Jaoui, M., Pye, H. O. T., Hu, W., Day, D. A.,  
587 Campuzano-Jost, P., Jimenez, J. L., Guo, H., Weber, R. J., de Gouw, J., Koss, A. R.,  
588 Edgerton, E. S., Brune, W., Mohr, C., Lopez-Hilfiker, F. D., Lutz, A., Kreisberg, N.  
589 M., Spielman, S. R., Hering, S. V., Wilson, K. R., Thornton, J. A. and Goldstein, A.  
590 H.: Monoterpenes are the largest source of summertime organic aerosol in the  
591 southeastern United States, *Proceedings of the National Academy of Sciences*,

592 201717513, doi:10.1073/pnas.1717513115, 2018.

593

594

595

596

597

598

599

600

601

602

603

604

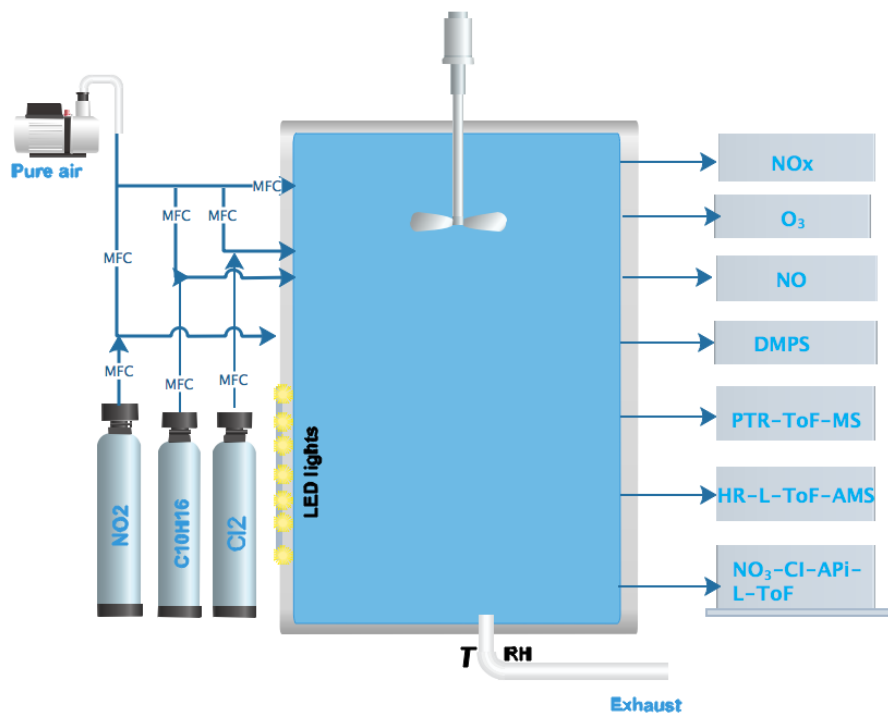
605

606

Figure and table captions

607

608



609

610 Figure 1 A schematic of the chamber setup and instruments used in the experiment.

611

612

613

614

615

616

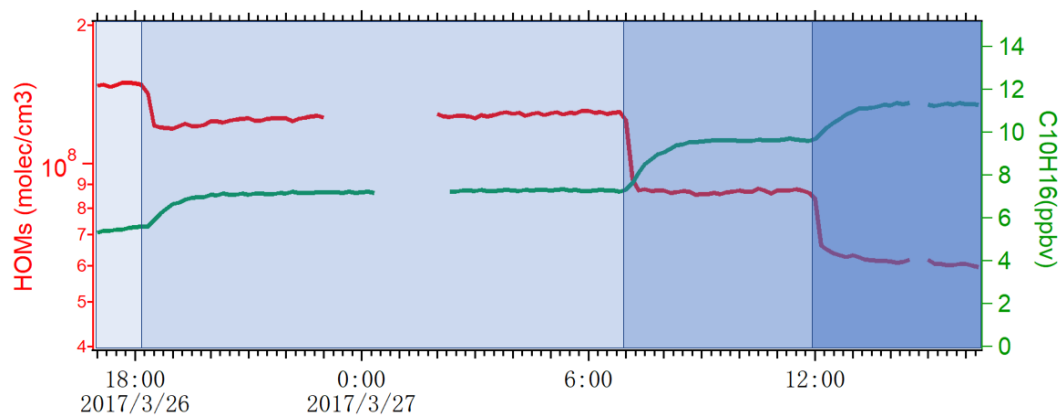
617

618

619

620

621



622

623

Figure 2. The variation of total HOM concentration and alpha-pinene during four  
 624 experiments where the 400 nm lights were decreased stepwise from 7 lights to 4, 2  
 625 and 1 light, respectively.

626

627

628

629

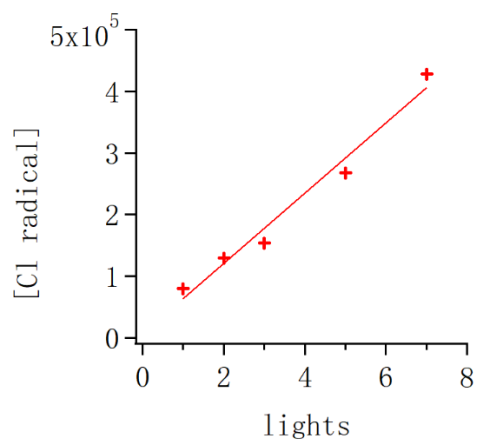
630

631

632

633





634

635

Figure 3. The variation of chlorine radical concentration as a function of lights. The

636

input alpha-pinene concentration was kept constant throughout the experiments.

637

638

639

640

641

642

643

644

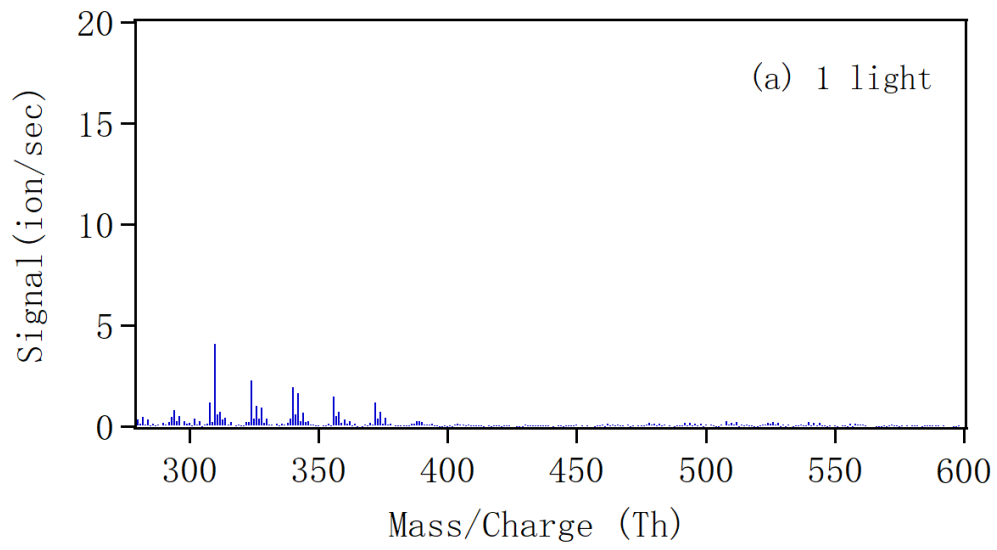
645

646

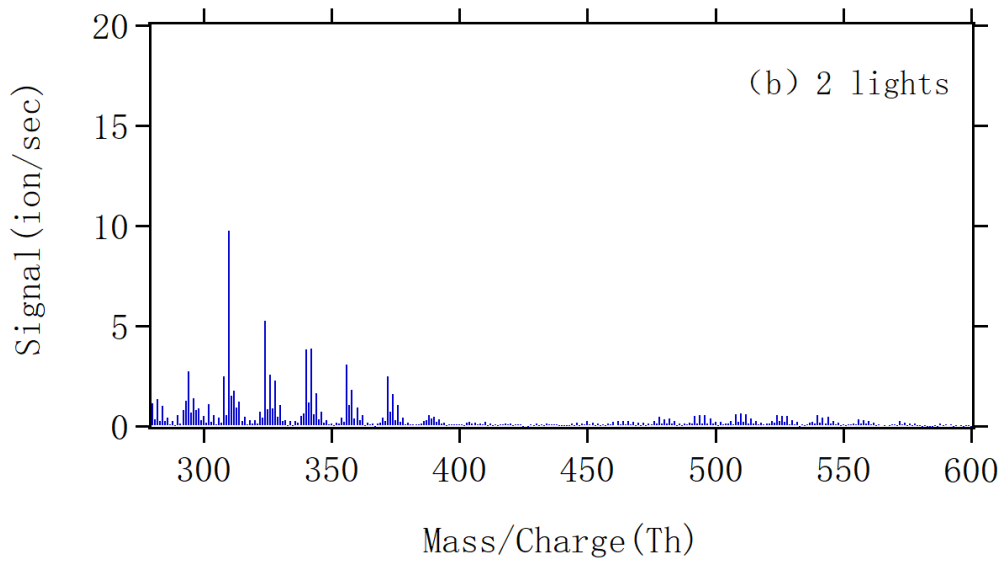
647

648

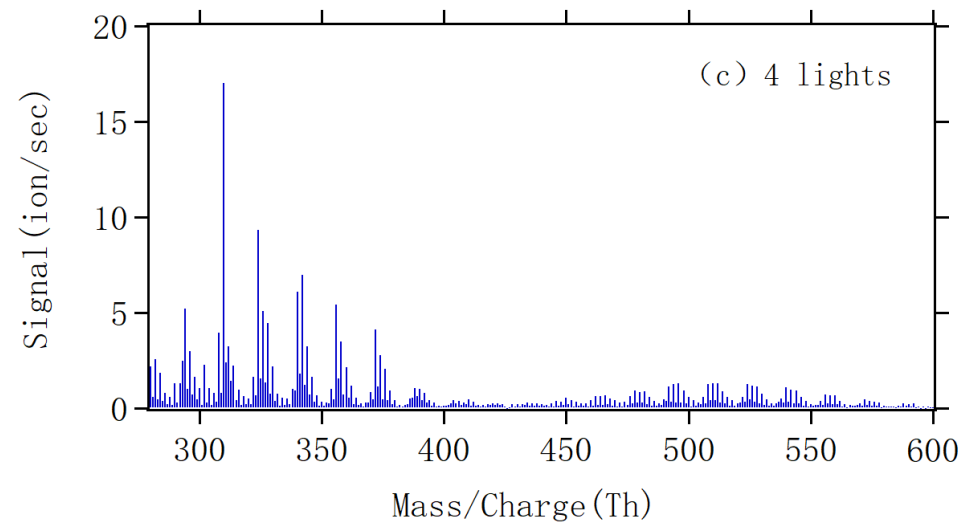
649



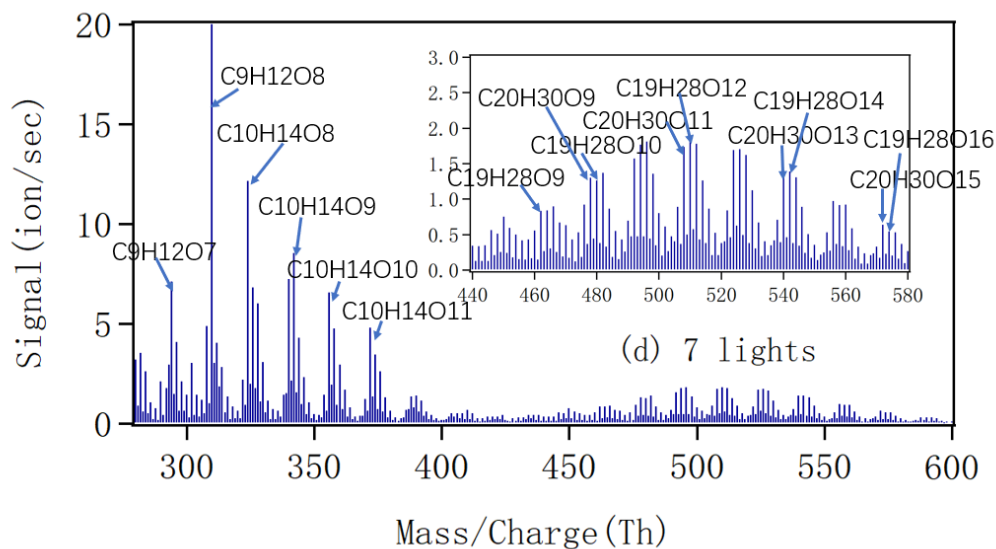
650



651



652



653

654

655 Figure 4. The mass spectra obtained by NO<sub>3</sub>-CI-API-TOF during steady state with 1(a),  
 656 2(b), 4(c) and 7(d) lights. All peaks are detected as clusters with NO<sub>3</sub><sup>-</sup>. The spectra are  
 657 plotted as unit mass resolution, with background signals removed, but the peak  
 658 identifications (labeled in panel d) are based on high resolution analyses. The spectra  
 659 correspond to the same four steady state conditions depicted in Fig. 2.

660

661

662

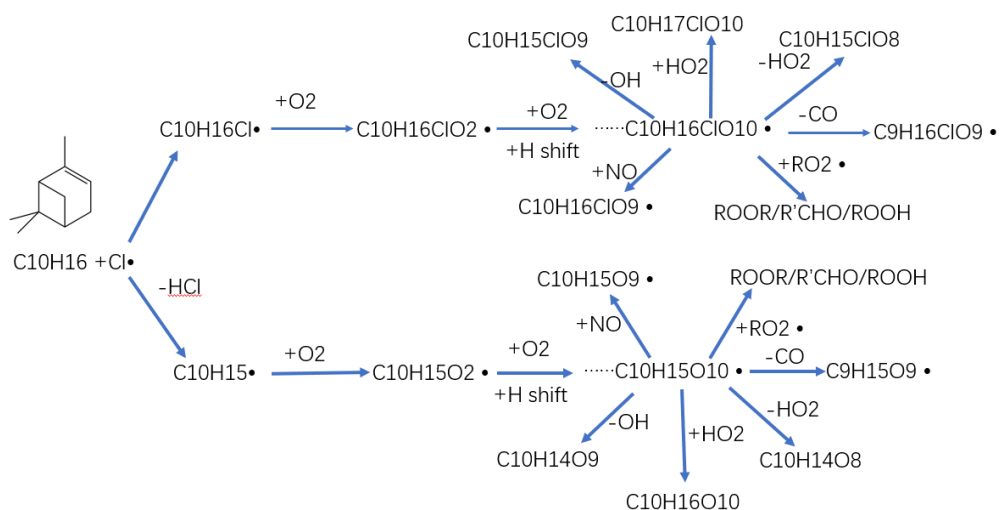
663

664

665

666

667



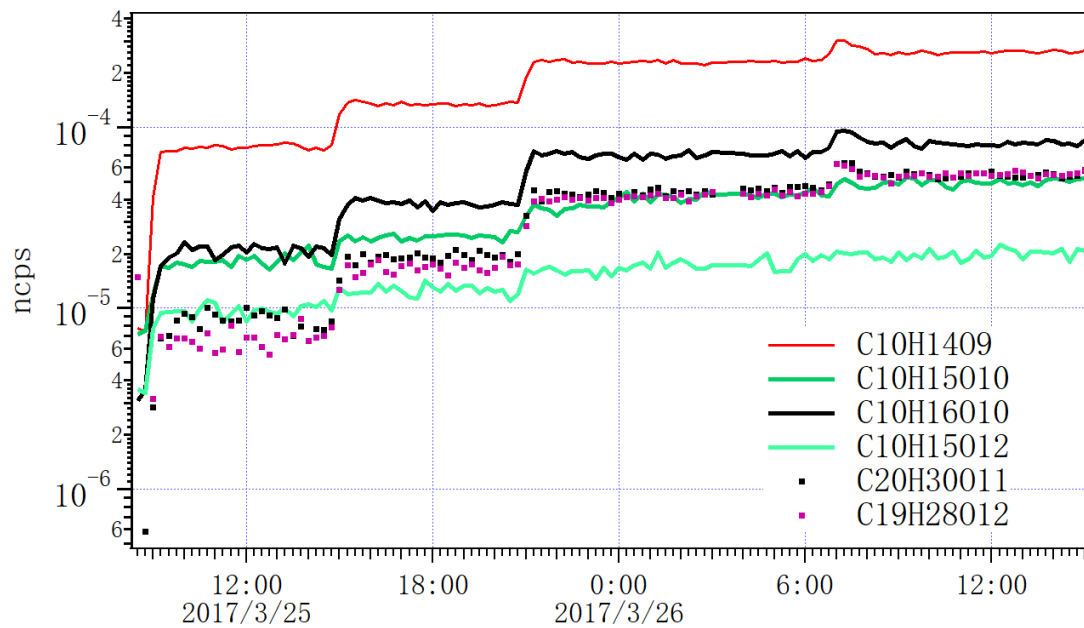
668

669 Figure 5. Proposed chemical pathways for chlorine radical oxidation of alpha-pinene,  
 670 and subsequent autoxidation and HOM formation. The upper path shows the chlorine  
 671 radical addition pathway, while the lower chain shows hydrogen atom abstraction  
 672 pathway. In both cases, initially a C-centered radical forms ( $C_{10}H_{16}Cl$  or  $C_{10}H_{15}$ ) to  
 673 which  $O_2$  adds to form an initial peroxy radical. This peroxy radical may then undergo  
 674 multi-step autoxidation to reach the example molecules  $C_{10}H_{16}ClO_{10}$  or  $C_{10}H_{15}O_{10}$   
 675 before termination.

676

677

678



679

680

681

682

683 Figure 6. Time series of selected closed-shell HOM monomers, dimers and an RO<sub>2</sub>

684 radical (C<sub>10</sub>H<sub>15</sub>O<sub>10</sub>) detected by NO<sub>3</sub>-CI-APi-TOF as the lights increased from 0 to 1,

685 2, 4 and 7.

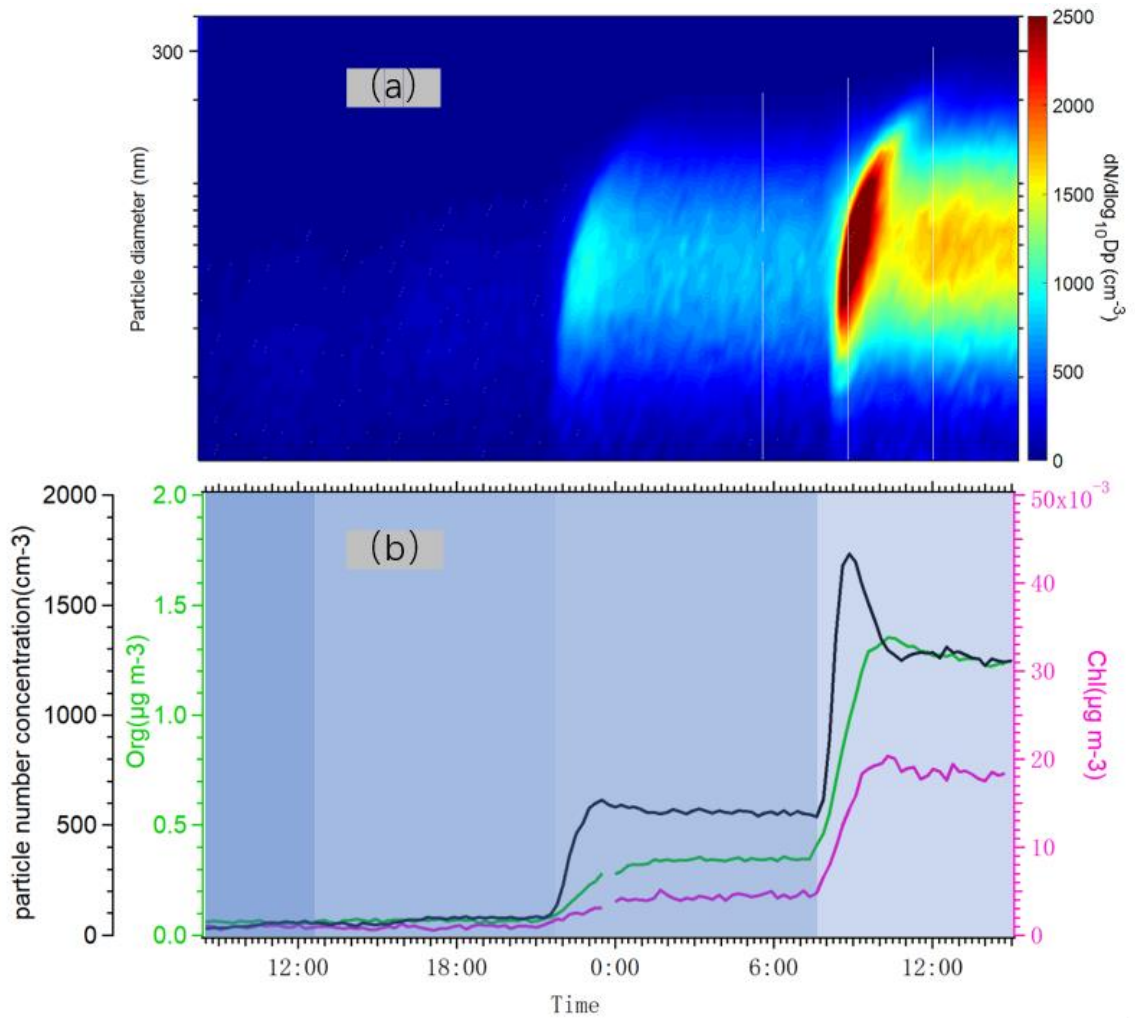
686

687

688

689

690



691

692

693 Figure 7. (a) Particle number size distribution measured by DMPS from 10 nm to

694 400nm when the lights varied from 1 to 2, 4 and 7. (b) Time series of total number

695 concentration (black) measured by DMPS, organic aerosol concentration (green) and

696 particulate chloride concentration (pink) measured by AMS.

697

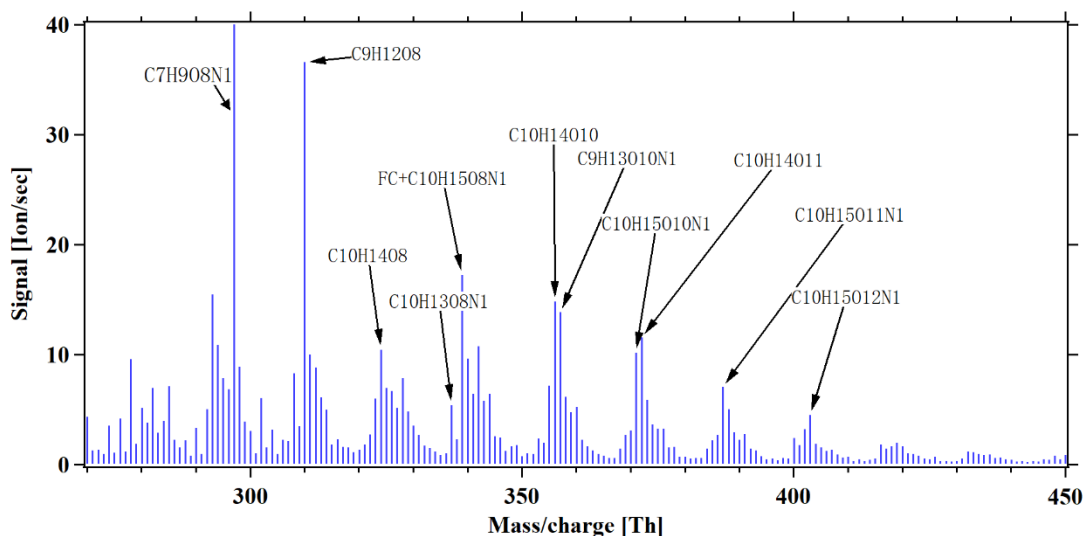
698

699

700

701

702



703

704 Figure 8. HOM mass spectrum during steady state alpha-pinene oxidation in the  
 705 presence of 10 ppb NO<sub>x</sub>, with 7 lights switched on. In addition to molecules detected  
 706 also in the experiments without NO<sub>x</sub>, several abundant **organic** nitrate peaks are formed.  
 707 Note that a fluorinated compounds (FC) overlaps with the organ nitrate C<sub>10</sub>H<sub>15</sub>O<sub>8</sub>N at  
 708 339Th. All peaks are detected as clusters with NO<sub>3</sub><sup>-</sup>.

709

710

711

712

713

714

715

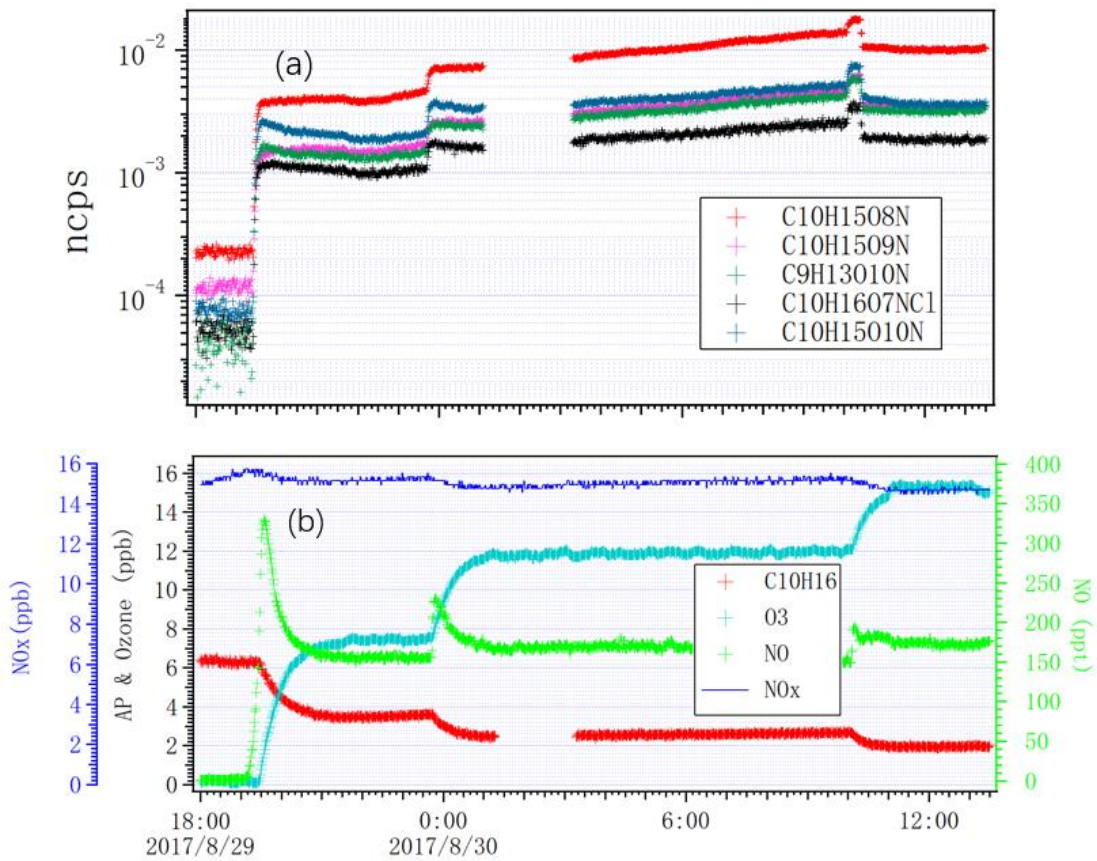
716

717

718

719

720



721

722

723 Figure 9. Time series of (a) selected HOMs measured by  $\text{NO}_3\text{-Cl-L-API-TOF}$  and (b)  
 724  $\text{NO}_x$ , a-pinene, ozone and NO, as the lights switched on from zero to 2, 4, and 7.

725

726

727

728

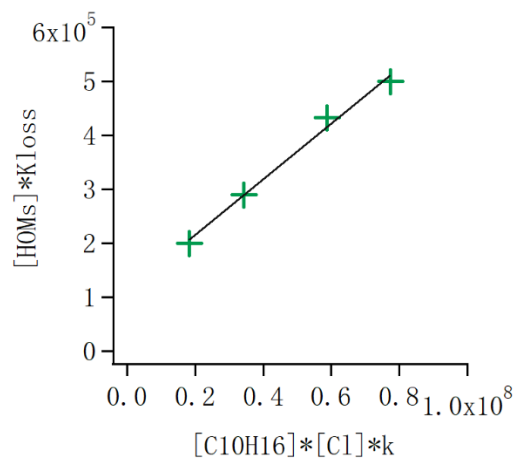
729

730

731

732





733

734

735 Figure 10. HOM loss rate ( $[HOM] \cdot K_{loss}$ ) as a function of the alpha-pinene  
 736 oxidation rate. In steady state the loss rate equals the formation rate, and thus  
 737 the slope of the points gives the molar yield of HOM from the alpha-pinene +  
 738 Cl reaction. The data corresponds to the conditions with 1, 2, 4 and 7 lights  
 739 switched on in the chamber, respectively. The slope indicates an average molar  
 740 yield of HOMs of 1.8%.

741

742

743